ELSEVIER

Biophysical Chemistry 98 (2002) 183–207

Biophysical Chemistry

www.elsevier.com/locate/bpc

# NO rebinding to myoglobin: a reactive molecular dynamics study

Markus Meuwly[a], Oren M. Becker[b,c], Roland Stote[a], Martin Karplus[a,c,*]

[a]*Laboratoire de Chimie Biophysique, ISIS UMR 7006, Universite Louis Pasteur, 67000 Strasbourg, France*
[b]*Department of Chemical Physics, School of Chemistry, Tel Aviv University Ramat Aviv, Tel Aviv 69978, Israel*
[c]*Department of Chemistry and Chemical Biology, Harvard University Cambridge, MA 02138, USA*

Received 11 January 2002; accepted 8 February 2002

**Abstract**

The rebinding of NO to myoglobin after photolysis is studied using the 'reactive molecular dynamics' method. In this approach the energy of the system is evaluated on two potential energy surfaces that include the heme–ligand interactions which change between liganded and unliganded myoglobin. This makes it possible to take into account in a simple way, the high dimensionality of the transition seam connecting the reactant and product states. The dynamics of the dissociated NO molecules are examined, and the geometrical and energetic properties of the transition seam are studied. Analysis of the frequency of recrossing shows that the height of the effective rebinding barrier is dependent on the time after photodissociation. This effect is due mainly to protein relaxation and may contribute to the experimentally observed non-exponential rebinding rate of NO, as has been suggested previously. 

*Keywords:* Myoglobin; Rebinding reaction; Reactive molecular dynamics

## 1. Introduction

Hemoglobin and myoglobin are the biological transport and storage systems for oxygen. Due to their physiological importance, the interaction of these proteins with their ligands ($O_2$, CO and NO) has been extensively studied both experimentally [1–9] and theoretically [8–19]. Moreover, attention has focused recently on the more general interaction of NO with heme proteins because of its wide range of biological functions. They include inhibition of mitochondrial respiration, inhibition of the enzyme ribonucleotide reductase and neurotransmission in the brain [20–22]. In many cases, NO binding to iron atoms in both heme and non-heme proteins seems to be involved. An important structural feature of both hemoglobin and myoglobin is that the binding and dissociation of the ligand induces a conformational change in the heme group [23]. Studies on model compounds and in proteins have shown that the five coordinate (unliganded) heme is domed with the iron atom out of the porphyrin plane, while the six coordinate (liganded) heme group is essentially flat (with some 'ruffling') and the iron atom is in or very near the heme plane. The change in the structure of the heme group has been shown to be the first

*Corresponding author. Tel.: +33-3-9024-1560; fax: +33-3-9024-1562.
*E-mail address:* marci@tammy.harvard.edu (M. Karplus).

0301-4622/02/$ - see front matter 
PII: S0301-4622(02)00093-5

step in the tertiary structural alterations induced by ligation of myoglobin and hemoglobin [24–26]; in hemoglobin, the tertiary change is coupled to the quaternary transition involved in the modulation of ligand binding.

Experimental studies of the rebinding of CO after photo-dissociation at different temperatures have shown that the superficially simple rebinding reaction is surprisingly complex [1–9,27]. The room temperature rebinding of CO is approximately exponential (with a time constant of 100 ns), while at low temperatures the rebinding is non-exponential in time and varies in a non-Arrhenius fashion with temperature. [1,4,5,7,28]. This behavior has been attributed to a distribution of barrier heights for the rebinding reaction in the effectively frozen protein [1,5,12,14]. This assumes that the relaxation of the protein at low temperatures is slow, relative to the rebinding reaction, so that the system is inhomogeneous with each protein molecule having a different barrier for rebinding. A range in barrier heights from approximately 2 to 10 kcal/mol has been inferred [12,14]. As yet, no single molecule experiments have been reported to verify this model. The rebinding of NO to Mb after photodissociation occurs on a much faster time scale and is non-exponential even at room ternperature [2,8,9,29]. The measured rebinding rate can be fitted either to a double exponential (28 and 280 ps components) or to a power law (with a 33 ps time scale) [8]. Femtosecond laser spectroscopy has shown that the photodissociation of MbCO, and probably also of MbNO, occurs in less than 300 fs [3,6]. For MbNO there are no experimental data concerning the temperature dependence of the rebinding from which information about the barrier can be obtained. However, the fact that the rebinding has a subnanosecond time scale indicates that the effective barrier is low, much lower than that for CO.

Because the rebinding of NO takes place in picoseconds at room temperature, it is on the same time scale as the fluctuations of the protein [11]. Therefore, it has been suggested [8] that for NO at room temperature, the non-exponential behavior is due to a time-dependent barrier, which increases as the iron moves out of the heme plane and the protein relaxes towards its unliganded equilibrium structure. A simple representation of such a time-dependent barrier $E(t)$ can be introduced into the Arrhenius equation by writing [8]

$$k(t) = A\exp^{-E(t)/RT} \quad (1)$$

with

$$E(t) = (E_0 - E_{eq})\exp^{-\kappa t} + E_{eq} \quad (2)$$

where $k(t)$ is the rate 'constant' for rebinding, $\kappa$ is the rate constant for the variation in the barrier height from its initial value, $E_0$, after photodissociation to its equilibrium value, $E_{eq}$. In deoxymyoglobin for NO rebinding, experimental values for the parameters are $A = 2.5\times10^{10}$ s$^{-1}$, $\kappa = 1.5\times10^{10}$ s$^{-1}$, $E_0 = 0.027$ kcal/mol and $E_{eq} = 1.2$ kcal/mol. These values correspond to an initial ($t = 0$) rebinding time constant of 42 ps and a final ($t = \infty$) time constant of 300 ps. Similar values were obtained for NO rebinding to hemoglobin [8].

There have been many molecular dynamics simulations of myoglobin because it has become a model system for the understanding of protein motions [11]. Many of these simulations have focused on equilibrium fluctuation and their temperature dependence [15,30,31]. Another series of simulations have been concerned with the exit of the ligand from the heme pocket [8,9,13,16,17,32,33]. Also, the heme relaxation after photodissociation has been studied by molecular dynamics simulations. It has been shown that the out-of-plane motion of the heme iron has a fast component [8,13] on a subpicosecond time scale (50–300 fs), during which the iron moves to approximately two-thirds of its distance in unliganded myoglobin, and a slower component on a 10 ps time scale; the latter is associated with heme doming and its interaction with the protein [8,33]. Over the 100 ps range of the simulations [33], the non-exponential relaxation of the iron distance from the mean porphyrin plane can be fitted by a power law or a stretched exponential.

The shift in frequency after photodissociation of a heme charge transfer band in MbCO at 760 nm has been associated with iron out-of-plane motion [13,34]. The timescale of the frequency shift has been shown to correspond to the iron out-of-plane motion over the range of the simulations (100 ps)

[35]. Experimentally, the non-exponential behavior of the charge transfer shift continues to nanoseconds [35]. The agreement between experiment and simulations over the time scale of the latter confirms the existence of the non-exponential relaxation [33,35].

Interestingly, the slow non-exponential phase of the iron out-of-plane motion has not been observed in two other simulations of photodissociation and rebinding [18,36]. The reason for this difference is not clear. One possible source is the somewhat different potential energy parameters used to describe the system. Since the non-exponential phase of the iron motion was not observed in these simulations, they were not able to determine whether it was related to the rebinding process. This is an aspect which is investigated in the present study. Although the non-exponential out-of-plane motion of the iron on the time scales of the rebinding is in accordance with the model of Petrich et al. [8], simulations of the actual rebinding process are needed. In the present study we introduce a treatment of the rebinding process with emphasis on the characteristics of the binding region.

There are two types of approaches that can be used to determine the potential energy surface for reactions involving bond-forming and bond-breaking in complex macromolecular systems. In one, the (adiabatic) potential energy surface for the reaction is determined by a combined quantum-mechanics/molecular-mechanics approach (QM/MM); the other method is based on coupled multiple surfaces that are described by pure molecular mechanics. In the QM/MM treatment [37–40], the system is partitioned into two parts. The reacting atoms are treated by quantum mechanical methods (e.g. AM1 or higher quantum mechanical level) and the rest of the system is treated by molecular mechanics; the coupling terms between the two parts of the system arise from electrostaticized and van der Waals interactions in cases where the QM and MM region are not part of the same molecule [40]; if they are, links between the QM and MM portions in the same molecule have to be introduced. This method has been applied to reactions in solution and in enzymes. The utility of the approach is limited by the time required for the parts of the system that are treated quantum mechanically. Very few dynamical simulations have been performed except for cases where the quantum mechanical part has been represented in a simplified form; an early example considered the isomerization dynamics of ethylene [41] and more recent examples were applied to enzymatic reactions [42].

An alternative approach treats the chemical reaction as a surface crossing between two molecular mechanics surfaces. One corresponds to the reactant state and the other to the product state. This method is suitable for non-adiabatic reactions (i.e. reactions where two electronic states are involved, as in the surface hopping model of Tully [43]), but it can also be used for adiabatic reactions with weak coupling between the reactant and product states. An early example based on this approach was used in trajectory calculations of the gas phase reaction, $K + Br_2 \rightarrow KBr + Br$ where simple molecular mechanics potential functions were used for the reactants surface (K, $Br_2$) and the product surface (KBr, Br) and an empirical exponential switching function was introduced to represent the coupling between the two surfaces [44]. While the surface coupling treatment is less 'exact' than the QM/MM approach (the surfaces and the coupling terms are usually empirical), the advantages include application and the speed of simulations. An approach of this type is the empirical valence bond method popularized by Warshel et al. [45]. Moreover, experimental information can be introduced in a straightforward manner when available. Such an approach, which has been called 'morphing potential' has been applied to small, non-reactive systems to yield potential energy surfaces of spectroscopic accuracy [46]. From this point of view, Mb + NO is a candidate for extending the morphing potential method to reactive macromolecular systems.

In the present paper, we use a special version of the two-surface approach and employ it to study the geometric and energetic characteristics of the rebinding of NO to myoglobin. In particular, we examine the dependence of the barrier crossing rate on the time after photodissociation has taken place. The two-surface model is particularly appropriate for the rebinding reaction of NO to the iron

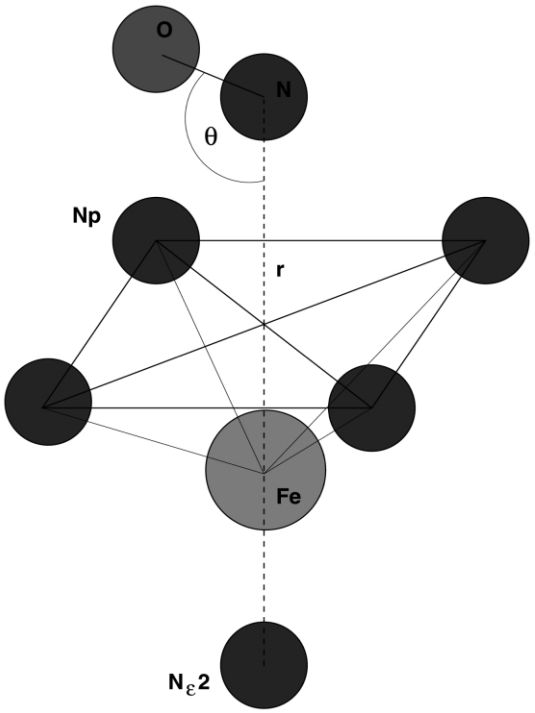


Fig. 1. The subsystem of MbNO used in the calculation (see text). It consists of the NO ligand, the Fe atom, the four pyrrole N atoms from the heme group and the N$\varepsilon$2 atom of the proximal histidine 93. The N–Fe–N$\varepsilon$2 axis is essentially linear and perpendicular to the plane of the four pyrrole nitrogens.

of the heme group because a 'surface crossing' is involved. Within 300 fs after photo dissociation the 'reactant' heme protein iron and NO are on the repulsive potential surface that corresponds to a high spin iron ($S=2$) and an NO molecule with $S=1/2$. After the rebinding reaction, the MbNO product has $S=1/2$. Although a spin transition is involved the reaction is assumed to be adiabatic, because spin-orbit coupling is expected to be strong [47]. Recently, the potential energy surface for the interaction of CO with a histidine-linked heme group has been calculated by high-level ab initio methods [48] and a corresponding study of NO is in progress; we discuss this further below.

Section 2 describes the model used for the potential energy surfaces and the method used for the molecular dynamics simulations. The results are presented in Section 3. A concluding discussion is given in Section 4. Appendices A and B list the molecular mechanics parameters of interest and describe a sensitivity analysis of dependence of the kinetics on some of their values.

## 2. Methods

### 2.1. Interaction potential for MbNO and Mb+NO

The global potential energy surface for MbNO is a function of the co-ordinates of all atoms involved. For the present model it was assumed that only a subset of all atoms—the 'active region'—directly participates in the reaction. The atoms which form this 'active region' are shown in Fig. 1. Interactions between these atoms are described by two different potentials; $V_{\text{unbound}}$ and $V_{\text{bound}}$ while the remaining interactions between atoms outside the active region are identical.

Both potential energy manifolds, $V_{\text{unbound}}$ and $V_{\text{bound}}$) for the reaction contain 12 terms (see Table 1) for the active region in which they differ. One manifold is for the reactant (unbound) state and the other for the product (bound) state after the photodissociation has taken place. The transition from the bound state ($^2A$, which is the lowest energy state for NO close to the heme iron), to the unbound state ($^4A$, which is the lowest energy state at infinite separation), is induced by photodissociation. The following two representations were chosen:

Table 1
The energetic terms included in the partial energy manifolds

| | | |
|---|---|---|
| Bound | | |
| Bonds | Fe–N | Morse |
| Angles | Fe–N–O | Harmonic |
| | N–Fe–Np | Harmonic |
| | N–Fe–N$\varepsilon$2 | Harmonic |
| Dihedrals | O–N–Fe–N$\varepsilon$2 | Cosine |
| | O–N–Fe–Np | Cosine |
| Unbound | N and O with Fe | VDW and electrostatic |
| | N and O with Np | VDW and electrostatic |
| | N and O with N$\varepsilon$2 | VDW and electrostatic |

Atom definitions as in Fig. 1.

Table 2
Summary of the potential energy parameters that characterize the NO interactions with the heme

| | | | |
|---|---|---|---|
| NO three point model | $q_N = -0.250e$<br>$q_O = -0.345e$<br>$q_{com} = 0.595e$ | $\varepsilon_N = 0.20$ kcal/mol<br>$\varepsilon_N = 0.16$ kcal/mol | $r_N = 2.00$ Å<br>$r_N = 2.05$ Å |
| Multipole moments | 3-pt model | Comparison | |
| $\mu_z$ | 0.153 D | 0.159 D (experiment) | |
| $Q_{zz}$ | 0.930 D Å | 1.165 D Å (ab initio) | |
| N–O bond | | | |
| in MbNO | $r_{eq} = 1.141$ Å | $k = 1653$ kcal/mol/Å$^2$ | Harmonic |
| in the Gas Phase | $r_{eq} = 1.151$ Å | $k = 2295$ kcal/mol/Å$^2$ | Harmonic |
| Fe–N bond | $r_{eq} = 1.740$ Å<br>$\beta = 3.2$ Å$^{-1}$ | $D_e = 30$ kcal/mol | Morse |
| Fe–N–O angle | $\theta_{eq} = 134°$ | $k = 70$ kcal/mol/rad$^2$ | Harmonic |
| Repulsive Fe–N | $C = 10$ kcal/mol | $V(r) = C\left(\frac{r}{r_{eq}}\right)^{-12}$ | |

$$
\begin{aligned}
V_{\text{bound}} = {} & D_e[e^{-2\beta(r-r_{\text{eq}})} - 2e^{-\beta(r-r_{\text{eq}})}] \\
& + k_{\text{Fe-N-O}}(\theta-\theta_{\text{eq}})^2 \\
& + \sum_{i=1}^{4} k_{\text{N-Fe-Np}_i}(\theta-\theta_{i\text{eq}})^2 \\
& + k_{\text{N-Fe-N}\varepsilon 2}(\theta_5-\theta_{\text{eq}})^2 \\
& + \sum_{i=1}^{4} k_{\text{O-N-Fe-Np}_i}\cos(\phi_i - 4\phi_{i\text{eq}}) \\
& + k_{\text{O-N-Fe-N}\varepsilon 2}\cos(\phi_5-\phi_{i\text{eq}}) \qquad (3)
\end{aligned}
$$

and

$$
\begin{aligned}
V_{\text{unbound}} = {} & \sum_{A=\text{Fe,Np,N}\varepsilon 2} (V_{LJ}(r_{\text{N}-A}) + V_{\text{Coul}}(r_{\text{N}-A})) \\
& + \sum_{A=\text{Fe,Np,N}\varepsilon 2} (V_{LJ}(r_{\text{O}-A}) \\
& + V_{\text{Coul}}(r_{\text{O}-A})) \\
& + \sum_{A=\text{Fe,Np,N}\varepsilon 2} V_{\text{Coul}}(r_{\text{CM}-A}) \qquad (4)
\end{aligned}
$$

Here, $r$ is the N–Fe distance, $\theta$ the Fe–N–O angle, $\theta_i$ and $\theta_5$ the N–Fe–Np$_i$ and N–Fe–N$\varepsilon$2 angles, and $\phi_i$ and $\phi_5$ the O–N–Fe–Np$_i$ and O–N–Fe–N$\varepsilon$2 dihedral angles. Co-ordinates with the subscript eq signify equilibrium values for the respective co-ordinate. In Eq. (4), $A$ is a summation index over all the atoms given under the sum.

The total potentials used for the simulations have the form

$$V^{\text{tot}}_{\text{bound}} = V_{\text{bound}} + V_{\text{protein}}$$

and

$$V^{\text{tot}}_{\text{unbound}} = V_{\text{unbound}} + V_{\text{protein}} \qquad (5)$$

In Eq. (5), $V_{\text{protein}}$ is the CHARMM22 potential which was used for the remaining part of the protein, including the heme. In $V_{\text{unbound}}$ the terms $V_{LJ}$ and $V_{\text{coul}}$ are the Lennard–Jones and electrostatic interactions from the CHARMM22 potential [49]. The additional term, $V_{\text{Coul}}(r_{\text{CM}}-A)$, is the interaction between the charge at the center of mass of NO and the surrounding atoms; this three-point model for NO is described below and the parameters are given in Table 2.

The two reduced potential energy surfaces encompass the atoms shown in Fig. 1 and include all energetic contributions to the reaction apart from an overall shift $\Delta$ of the total energy. The constant $\Delta$ is the shift between the bound and unbound potential manifold at infinite separation ($R = \infty$) (see Fig. 2). Thus, $\Delta$ corresponds to the electronic separation of the $^2A$ and $^4A$ potential energy surfaces. Since the ligand is at infinite separation, the results obtained recently for a model consisting of a heme, histidine and a CO molecule with an ab initio density functional calculation provide an estimate of approximately 5 kcal/mol [48].

Because the unbound and bound energy surfaces have different zeroes of energy that are implicit in

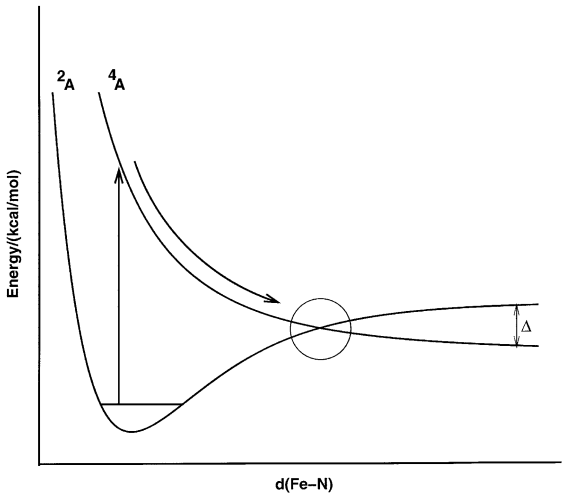


Fig. 2. Schematic one-dimensional cross-sections along the Fe–N co-ordinate through the multi-dimensional interaction manifolds used in the calculation. This cut shows the two Fe–N interaction potentials: the bound Morse potential; and the dissociative repulsive interaction. The parameter Δ is the energy gap ($R \rightarrow \infty$) between the two surfaces (see text).

the molecular mechanics energy function, Δ was estimated in the following way to obtain consistent results: the displacement between the two partial potential surfaces, $V_{\text{bound}}$ and $V_{\text{unbound}}$, at infinite ligand separation is due to the internal heme parameters which change from the unliganded to the liganded system; they are not included in $V_{\text{bound}}$ and $V_{\text{unbound}}$, though they are included in $V^{\text{tot}}_{\text{unbound}}$ used for the simulations (see below). The internal heme parameters are the Fe–N$\varepsilon$2 and Np–Fe bonds and the Np–Fe–Np and Np–Fe–N$\varepsilon$2 angles; the parameters used for the bound and unbound heme group are given in Table 3. To estimate their contribution to the energy, molecular dynamics calculations of 25 ps in length for a fully solvated, equilibrated bound and unbound system were run at 300 K, see Section 2.2. It was found that the internal heme energy contributed by these terms for the unbound Mb+NO is $11.5 \pm 1$ kcal/mol higher than that of bound MbNO. Thus, the energy difference is of the same order but approximately twice the ab initio value, both of which are approximate. The value of $\Delta = 11.5$ kcal/mol is used in the present calculations for consistency with the parameters of the force field. We investigate the sensitivity of the results to changes in the potential parameters for the unbound heme in Appendix B since these parameters are less well known.

To perform the rebinding study it was necessary to develop parameters that describe the NO ligand and its interactions with the heme in its bound and unbound state. For the unbound ligand, standard gas phase parameters were used for the NO bond with a harmonic force constant. A three-site model, analogous to that developed previously for CO [17], was introduced to represent the non-bonded interactions so as to account for both the small dipole moment and larger quadrupole moment of NO. For the bound state, the NO bond was assumed to be somewhat weaker than that in the gas phase. Details of the approach used to determine the parameters are given in the Appendix A. The parameters are summarized in Table 2. The other parameters were taken from previous work on liganded ('oxy-') and unliganded ('deoxy-') MbCO [8,31].

We introduce a version of the two-surface approach that accounts for the fact that most of the protein is not directly involved in the reactive dynamics. In a manner analogous to that used in a QM/MM treatment [40], the system is partitioned into a reaction region and an environment. Only terms directly involved in the reaction are different for the two surfaces [see Eqs. (3)–(5)]. Thus, to identify the transition seam it is possible to restrict the calculation to the terms that change

Table 3
Potential parameters used for five- and six-coordinated heme

| Parameter | Five-coordinated | | Six-coordinated | |
|---|---|---|---|---|
| | $r$ (Å) | $k$ (kcal/mol) | $r$ (Å) | $k$ (kcal/mol) |
| Bonds | | | | |
| NPH–FE | 2.10 | 272.2 | 1.958 | 270.2 |
| NE2–FE | 2.10 | 65.0 | 2.20 | 65.0 |
| | $\theta_e$ (°) | $k$ (kcal/mol) | $\theta_e$ (°) | $k$ (kcal/mol) |
| Valence angles | | | | |
| NPH–FE–NPH | 90.0 | 80.0 | 90.0 | 14.39 |
| NE2–FE–NPH | 107.0 | 50.0 | 90.0 | 50.0 |

as a result of the reaction; all other terms in the potential energy function cancel exactly [Eq. (5)]. Instead of calculating the energy on two full potential energy surfaces, the method used reduces the calculation to a single surface plus a small fraction of another surface. Since the force and energy calculations usually take most of the total computation time in molecular dynamics simulations, this partitioning scheme can lead to a considerable reduction in computer time. The high dimensionality of the transition seam, which has been shown to be important for many reactions involving proteins, is retained [50].

### 2.2. Preparation of the system

The starting configuration for the simulations was the X-ray structure of MbCO to which hydrogen atoms were added [23,49]. As the rebinding reaction is confined to the heme pocket we used the stochastic boundary method to increase computational efficiency [51–53]. The application of this method is similar to that employed in a previous study of MbCO photodissociation [17]. A 12-Å active site region was used and the reservoir region was neglected. A 16-Å sphere of TIP3P water molecules was added around the center of the full system (defined by the center of the four Np atoms, see Fig. 1) by three random overlays of an equilibrated sphere of water molecules [54]. Water molecules closer than 2.8 Å to a neighboring heavy atom were removed. Each overlay was followed by 20 ps of Langevin dynamics for equilibration of the water molecules during which MbNO was kept fixed [49]. The active site region of the system is shown in Fig. 3a,b.

A total of 178 water molecules were added resulting in a total of 2532 heme protein atoms, the NO ligand and 534 water atoms in the simulation. The solvent molecules were constrained relative to the center by a solvent boundary potential with a radius of 16 Å and all bonds to hydrogen atoms were constrained using the SHAKE algorithm [55]. The non-bonded interactions were truncated at a distance of 9 Å using a shift function for electrostatic interactions and a switch algorithm for van der Waals interactions [49]. A dielectric

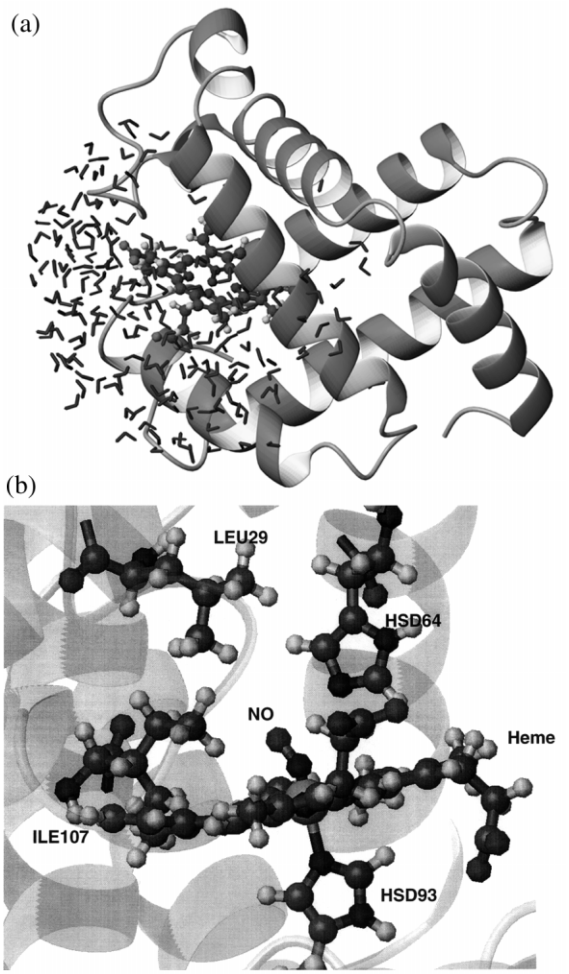


Fig. 3. (a) Representation of the simulated system: ribbon model for protein together with a ball-and-stick model of the heme and all water molecules (lines). The solvent sphere is covering the heme and the surrounding residues of the heme pocket. (b) Closer view of the heme pocket; the relevant residues are labeled. The iron atom is shown in green at the center and residue Phe43, also involved in the heme pocket, is not shown for clarity. The helices are shown as translucent spirals.

constant of one was used [49]. The reactive molecular dynamics (RMD) calculations were performed with the CHARMM program using the CHARMM22 all-atom representation [49].

To relieve strains the system was first minimized and then equilibrated for 80 ps at 300 K. The root-mean-square deviations of the equilibrated system from the X-ray structure were 0.34 Å for the

backbone atoms and 0.53 Å for all non-hydrogen atoms.

The dissociation was simulated by the 'sudden' approximation following a method used previously for MbCO photodissociation [8]. The Fe–N bond function was deleted, the bound potential energy surface was replaced by the unbound potential energy surface and a repulsive term between the iron and the ligand nitrogen atom was introduced. This repulsive potential is of the form

$$V(r) = C\left(\frac{r}{r_{eq}}\right)^{-12} \quad (6)$$

where $r$ is the Fe–N distance, $r_{eq}$ is the equilibrium distance of the Fe–N bond and $C = 10$ kcal/mol is an energy parameter. It mimics the repulsive excited state to which the Fe–N bond is pumped by the photodissociating laser pulse [6,35]. During the time that the direct repulsion is in effect the non-bonded interactions of the NO ligand with the heme gate [i.e. the terms in Eq. (4)] are not included so that the system is represented by $V_{protein} + V(r)$. Only when the bond is fully dissociated [and the special term, Eq. (6), is turned off] are these non-bonded interactions re-introduced into the simulation.

The increase in the potential energy of the simulated system upon introducing the above changes to mimic photodissociation is comparable to the experimental excitation energy. For example, in the simulations that started from the configuration obtained after 75 ps of equilibration the potential energy before excitation was equal to $-3509.19$ kcal/mol and the potential energy of the 'excited state' was $-3488.02$ kcal/mol; i.e. a difference in energy of 21.17 kcal/mol. Adding the Fe–N bond energy, which is $\approx 30$ kcal/mol, we obtain an excitation energy of 51 kcal/mol. This value is in the range of photon energies used in the dissociation experiments where the wavelengths varied from $\lambda = 580$ nm (49 kcal/mol) to $\lambda = 353$ nm (81 kcal/mol) [35]. Similar values of the excitation energy were obtained for all trajectories; the values ranged between 50 and 60 kcal/mol.

### 2.3. Reactive molecular dynamics

The system is propagated on the potential energy surface of the unbound state (Mb + NO). The interaction between the heme and the unligated NO molecule as given by Eq. (4) is purely repulsive. This assumption is in accord with the high-level ab initio calculations for Mb + CO [48]. During the dynamics, the energies on the two partial manifolds [representing the bound (MbNO) and the unbound (Mb + NO) state] described above [Eqs. (3) and (4)] are continuously compared. If the energies of the two partial manifolds are equal, the system has reached a crossing point (the transition seam) and a transition can take place. This occurs whenever the sum of the energy on the bound manifold plus the constant $\Delta$ (see Section 2.1) is lower than the energy on the unbound (dissociated) manifold; i.e. when

$$E_{bound} + \Delta < E_{unbound} \quad (7)$$

where $\Delta = 11.5$ kcal/mol. The shift $\Delta$ affects the absolute value of the rebinding barrier and could be selected in such a way that the barrier height results in the experimental value for the rebinding rate (the peak rate is 0.02 $ps^{-1}$ for a power law fit of the absorbance [8]).

Whether a transition actually occurs depends on the nature of the system. We assume the adiabatic limit so that the crossing probability at the transition seam can be taken to be unity. Also, a recrossing to the unbound state can be neglected due to the rapid redistribution of the excess kinetic energy after crossing to the bound surface for this strongly coupled system. Consequently, we do not follow the system after it has performed the transition from the unbound to the bound state. We restrict ourselves to characterizing the transition seam and the time dependence of the possibility of recrossing.

A total of 20 simulations of 50 ps in duration on the unbound potential energy surface were performed and $V_{bound}$ Eq. (3) and $V_{unbound}$ Eq. (4) were compared during the trajectory. This trajectory length was chosen to sample adequately the rebinding reaction during the fast phase of the rebinding process, which is on a time scale of 28 ps [8]. It also makes it possible to determine

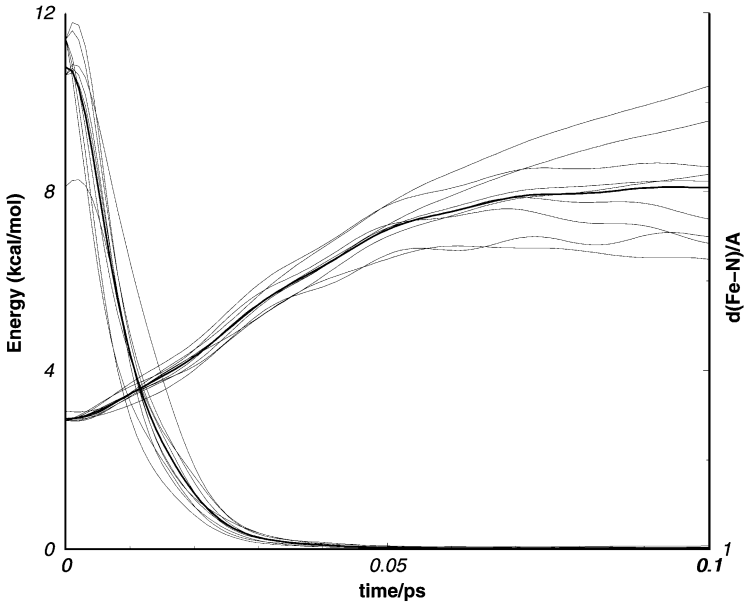


Fig. 4. Individual and average contribution from the direct dissociation potential [Eq. (6)] (solid line) and the average Fe–N distances (dashed line) during the first 100 fs of dissociation. The averages (thick lines) were taken over nine trajectories.

whether there is a coupling between the average iron out-of-plane position, which increases with time, and the non-exponential behavior observed for the NO rebinding reaction [8,33]. In addition, nine 500-ps trajectories were run. They were used to investigate briefly dynamical effects on a longer time scale.

The simulations were started from different configurations generated towards the end of the equilibration run (five trajectories each using the configuration at 65 and 70 ps, and 10 trajectories using the configurations at 75 ps) with different random velocities from a thermal distribution at 300 K assigned to the atoms prior to dissociation. As mentioned earlier, all simulations remained on the unbound potential without switching for the entire run; i.e. each curve crossing was recorded but the propagation continued on the unbound surface. The MbNO rebinding process occurs after the translation and rotation of NO are thermalized, and the subsequent times at which crossing is possible appear largely uncorrelated (see below). One important aspect of proceeding in this way is that crossings that take place at longer times after photodissociation are sampled more easily. Otherwise, many long trajectories would be required to obtain sufficient sampling for crossings at longer times so as to be able to correlate the heme relaxation after photodissociation with the rebinding rate.

## 3. Results

### *3.1. Mb–NO dissociation*

In previous simulations of MbCO dissociation it was found that the Fe–C bond breaks within 50–100 fs [1–9,17,56]. A fast initial relaxation of the iron out-of-plane motion was observed followed by a slower relaxation to the equilibrium value with oscillations around the equilibrium value. This result is in accord with heme visible absorption and CO infrared absorption measurements on the femtosecond time scale. The experiments are consistent with the presence of a free CO within a 300 fs delay after photodissociation [3,6]. Fig. 4 shows the results for photo dissociation of NO, which indicate that the direct interac-

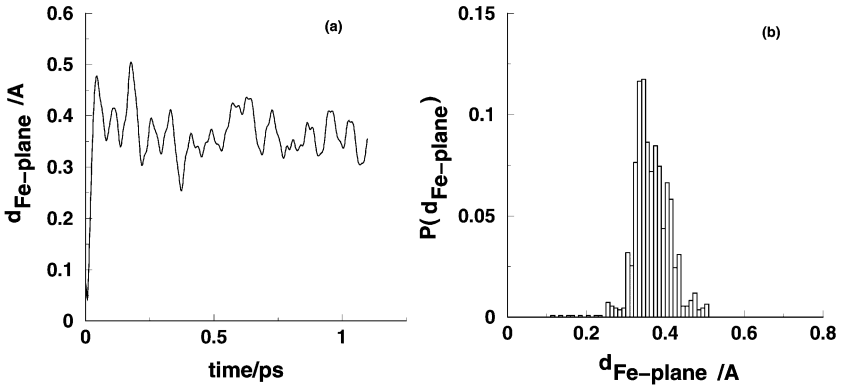


Fig. 5. (a) Average of the Fe–Np plane distance over 20 trajectories each of 1.1 ps in length. The initial 0.1 ps is the dissociation phase (with the term from Eq. (6)) followed by 1 ps of dynamics on the unbound potential energy surface. (b) The distribution of these distances with a binning of 0.01 Å.

tion becomes negligible after approximately 50 fs (40–60 fs depending on the trajectory). The average contribution of the dissociation potential [Eq. (6)] to the total energy after 50 fs was $0.05 \pm 0.02$ kcal/mol and it was reduced further to $0.01 \pm 0.005$ kcal/mol at 100 fs (all fluctuations are given in terms of a single standard deviation). Examination of the individual trajectories showed that those with initial momentum along the Fe–NO axis corresponding to bond contraction dissociated more slowly than those with bond stretching motion. After 100 fs the dissociation potential was turned off and the non-bonded interactions between the NO and the heme were re-introduced, as described in Section 2.

Starting from the vicinity of the equilibrium bond length (1.74 Å) the Fe–N distance increases to an average value of $2.7 \pm 0.25$ Å at 50 fs and it reaches $3.05 \pm 0.5$ Å when the dissociation term is turned off (100 fs). The distance continues to increase to approximately 4.5 Å at 200 fs. At this point, the ligand is close to the far side of the heme pocket where it is reflected and undergoes a motion within a confined region [57].

After photodissociation, the Fe atom moves out of the heme plane to a distance of approximately 0.35 Å, relative to the four pyrrole nitrogens and 0.5 Å relative to the heme heavy atoms within the first 50–100 fs of the simulation, in accordance with previous simulations. Fig. 5 shows the

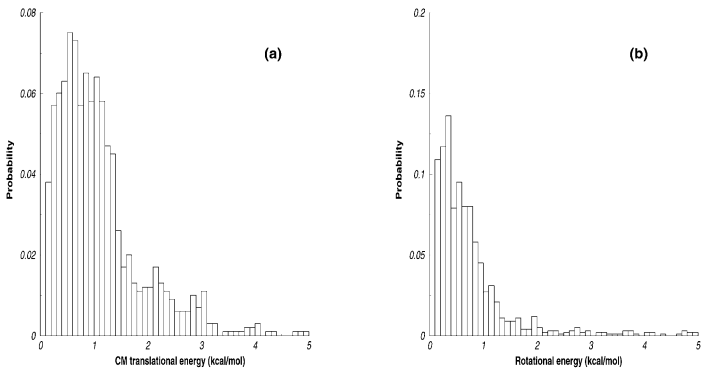


Fig. 6. Distribution of NO kinetic energy along a 50 ps trajectory following its dissociation from myoglobin. (a) Distribution of instantaneous center-of-mass translational energy; (b) distribution of instantaneous rotational energy.

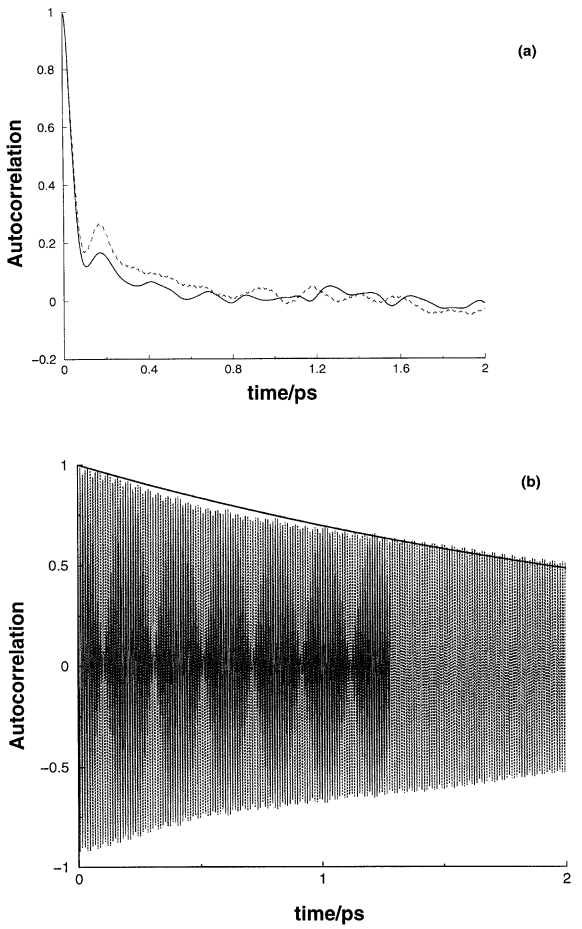


Fig. 7. Autocorrelation functions for different energy terms for the NO molecule after its dissociation from myoglobin. (a) The center-of-mass translational energy autocorrelation function (solid line) and the rotational energy autocorrelation function (dashed line), averaged over all trajectories. (b) The vibrational autocorrelation function (from a single trajectory). The solid line is a single exponential fit to the envelope with a relaxation time of 6.7 ps.

Fe–Heme distances for 1 ps of dynamics after photo dissociation together with the corresponding probability distribution. The distribution of the short time trajectories quickly evolves towards the average value for the Fe–Heme distance, which is 0.39 Å [58].

### *3.2. Mb–NO pocket dynamics*

After photodissociation is complete (see Section 2) the non-bonded interactions between the NO and the gate atoms (Fe and Np atoms) were reintroduced [see Eq. (4)]. In all trajectories, the average translational kinetic energy of the ligand center-of-mass was 0.9–1.0 kcal/mol at $t=0.2$ ps after dissociation; i.e. it was equal to the thermal value $\frac{3}{2}kT=0.9$ kcal/mol at 300 K. The thermalization is evident from the Maxwell–Boltzmann distribution of the translational energy (Fig. 6a). As expected, thermal fluctuations are as large as 3.5–4 kcal/mol. They generally last no more than 0.2 ps. Fig. 7a shows the autocorrelation function of the center-of-mass translational energy, averaged over all 20 trajectories. The correlation time for relaxation of the center-of-mass translational energy is approximately 200 fs. The oscillatory nature of the correlation function arises from collisions with the heme and the protein residues, analogous to what is observed in dense liquids.

The vibrational energy of NO behaves very differently from the translational and rotational energy. It was calculated from the projections of the velocities of the N and O atom along the intermolecular bond. The average vibrational energy from one run to the other varied between 0.58 and 1.65 kcal/mol. Since the kinetic energy is approximately half of the total NO energy, the NO ligands have 1.16–3.30 kcal/mol in that mode. The average potential energy varied between 0.4 and 1.5 kcal/mol. All these energies can be regarded as corresponding to the ground state $v=0$, since they are smaller than the vibrational energy spacing in NO ($h\nu=5.45$ kcal/mol) even if anharmonic effects are taken into account. This indicates that for a quantitative assessment of the NO vibrational motion a quantum mechanical treatment would be required. The autocorrelation function of the vibrational energy (Fig. 7b) is underdamped. The relaxation times, which were extracted from an exponential fit to the envelope of the correlation function, varied significantly from trajectory to trajectory and ranged from 2 to 17 ps. The high frequency mode in Fig. 7b is the NO vibration, which has a period of 17.5 fs, and the overall envelope corresponds to the damping. The intermediate envelope, at a period of approximately 200 fs, is an artifact reflecting the data

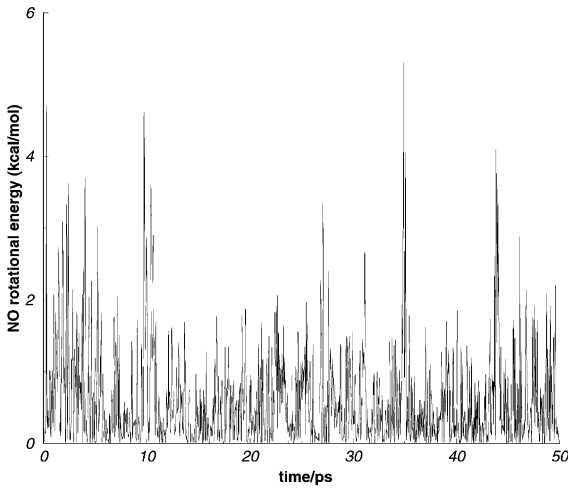


Fig. 8. The rotational energy of NO during 50 ps of dynamics on the unbound potential energy surface. The rotational energy has been calculated from the velocity components orthogonal to the NO bond (see text).

sampling frequency (the trajectory data were written out every 5 fs).

The rotational energy $T_{\mathrm{rot}}$ was calculated as the difference between the total kinetic energy and its translational and vibrational components. It thus, includes the vibrational-rotational coupling. The rotational energy also shows thermal behavior on average (Fig. 6b) and rapid decorrelation (Fig. 7a,b). In most trajectories, the average rotational energy of the ligand was 0.53–0.67 kcal/mol, which equals $kT$ at 300 K (Fig. 6b). Similar to the translational energy, the rotational energy shows significant fluctuations, which last for no longer than 0.2–0.3 ps and can be as high as 2.5–3.5 kcal/mol (there can be exceptional peaks up to 5 kcal/mol). It is important to note that while $kT$ is the mean thermal energy of a free rotor, the NO molecule is actually strongly hindered in its rotational motion. This can be seen in the correlation function of the rotational energy (Fig. 7b) which is overdamped. The decorrelation time is approximately 150 ps [6,17].

It is also possible to calculate a rotational energy $T_{\mathrm{rot}}^{\mathrm{ang}}$ from the two velocity components of NO orthogonal to the NO bond (Fig. 8). This gives a means to assess the magnitude of the coupling between the rotational and vibrational motion in NO. The average difference between $T_{\mathrm{rot}}^{\mathrm{ang}}$ and $T_{\mathrm{rot}}$ is $-0.08$ kcal/mol with the fluctuations in the range of $\pm 1$ kcal/mol. This is in accordance with the standard expression for rotational–vibrational energy levels of an anharmonic diatomic molecule for which the coupling constant is negative [59]. The coupling energy is approximately 10 times smaller than the rotational energy itself. This ratio is smaller than the ratio of the rovibrational coupling constant ($-0.0178$ cm$^{-1}$) and rotational constant (1.705 cm$^{-1}$) in NO [59]. However, quantitative agreement cannot be expected, in part because the rovibrational energy of NO should be treated quantum mechanically.

The total kinetic energy of the dissociated NO ligand is the sum of its translational, vibrational, rotational and coupling term and reflect the behavior described above. Fig. 9 shows a representative picture from one 50-ps trajectory for the three energy terms. The average total kinetic energy over 50 ps varies from one trajectory to another and ranges between $1.8 \pm 1.0$ and $3.2 \pm 1.6$ kcal/mol. These results are comparable to those from studies of the photo dissociation of CO from myoglobin [17].

The long-time behavior of the pocket dynamics was also investigated. It is of particular interest to compare the Fe–heme distance for the 20 trajectories (each 50 ps in length with varying initial conditions) with simulations of longer duration. Fig. 10 compares the distributions of the average Fe–heme distance for a 500-ps trajectory, and one 50-ps trajectory. The distributions of both trajectories are very similar to each other. Thus, the short and long trajectories sample a comparable distribution. The distribution of the average Fe–heme distance peaks at 0.4 Å which is close to the experimental value [8,58].

### 3.3. Mb–NO rebinding

To study the nature of the Mb–NO rebinding barrier we used the sampling enhancement approach described in Section 2. The system was propagated on the potential energy surface of the unbound state and the partial manifold calculations were used to identify possible crossing events.

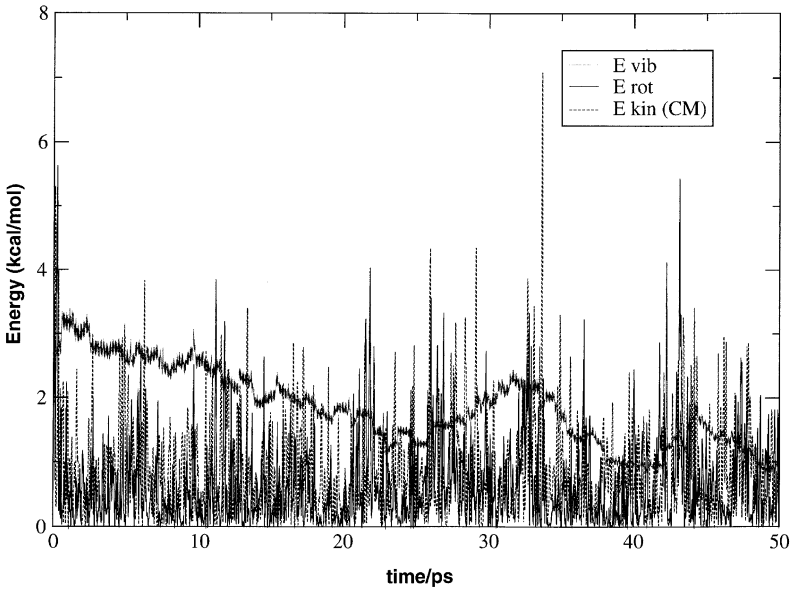


Fig. 9. All internal energy terms of the NO molecules for one typical 50 ps trajectory. Due to the rapid oscillation of the vibrational energy a running average over five neighboring points is shown. The rotational and translational energies are shown at every recorded time step.

Since both the translational and the rotational energy components of the ligand decorrelate very quickly (~200 fs, Fig. 7a) and the vibrational period is very short (17.5 fs, see also below), successive attempted crossing events along a single trajectory are expected to be uncorrelated. The local motions of the protein are expected to be on a relatively fast time scale, also contributing to the uncorrelated nature of successive attempts. The crossing attempts occur approximately every 1–3 ps. As described above, attempted crossings are characterized by the fact that the energy of the

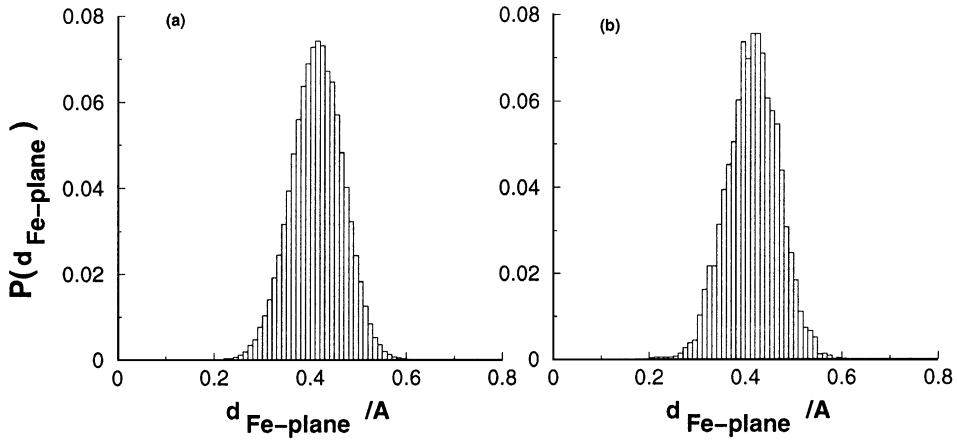


Fig. 10. Distribution of the Fe–Np plane distance for one 500 ps (a) and one 50 ps (b) trajectory on the unbound potential energy surface. This figure should be compared with Fig. 5.

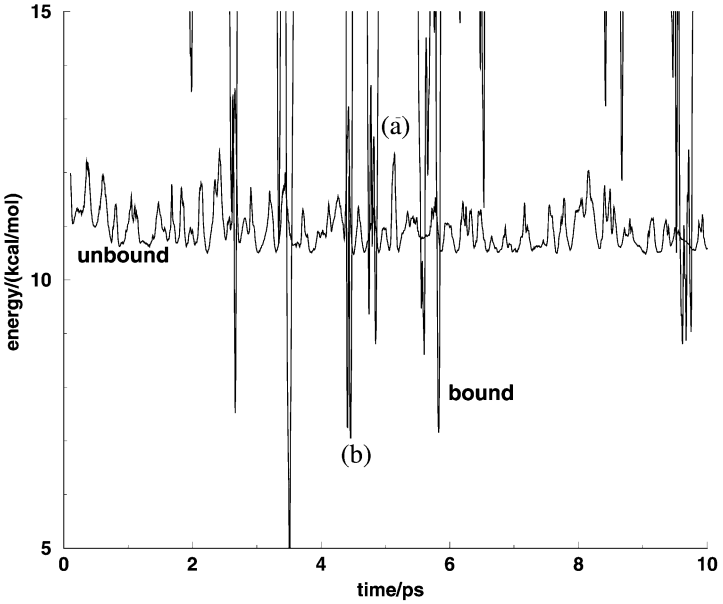


Fig. 11. The energy of the two partial manifolds—the bound state manifold (solid line) and the dissociated state manifold (dashed line)—during the first 10 ps of one trajectory. One high-energy configuration on the unbound surface, which does not lead to reaction (a) and one reactive configuration (b) are indicated. The large fluctuations in energy of the bound state, is mainly a consequence of the harmonic term for the Fe–N–O angle (see text).

bound (product) state is lower than the energy of the unbound (reactant) state (Eq. (6)).

The only energy component that shows long-time correlation is the NO vibration. However, we did not find any correlation between the NO vibrational energy and the curve crossing events, indicating that this mode is not significant in MbNO rebinding. The energies of the two partial manifolds, the bound and unbound state manifold, are shown in Fig. 11 (the figure shown is the first few picoseconds from one trajectory; similar results were obtained in all trajectories). Since the data shown correspond to only part of the energy, only the relative energies are significant.

The harmonic Fe–N–O angle term (Tables 1 and 2) is mainly responsible for the high bound-state energies when the system is away from the transition seam. Specifically, the linear Fe–NO configuration (which is 40° off the equilibrium angle) has an energy of 33 kcal/mol. Although this exaggeration of bound-state energies does not affect the values near the rebinding barrier, the angular contribution would be better described by a cosine function rather than by the harmonic function which we used [60,61].

The high energy spikes on the unbound manifold represent collisions of the NO with the heme. Although these collisions are candidates for crossing events we see from Fig. 11 that the collision frequency (several times per picosecond) is much higher than the crossing frequency (which is approximately one every 1–3 ps). Therefore, a collision [feature (a) in Fig. 11] is not sufficient for a reaction to take place. Additional requirements on the NO orientation must be met. The favorable reactive geometries correspond to the downward energy spikes on the bound state manifold [feature (b) in Fig. 11]. These configurations represent a NO molecule approaching the Fe atom in a favorable orientation with respect to the Fe–N–O angle. When the ligand–heme geometry differs significantly from the bound state geometry (e.g. when the molecule approaches with the O end) the interaction on the bound-state manifold is highly unfavorable.

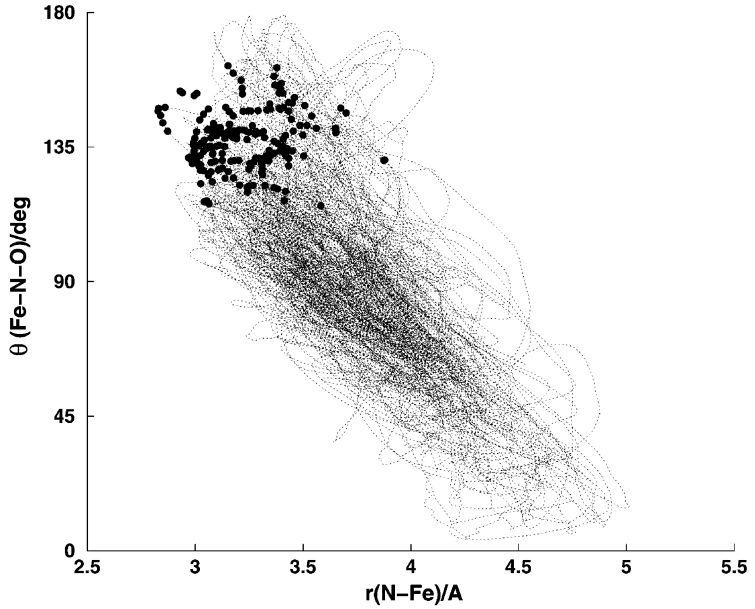


Fig. 12. MbNO rebinding barrier configurations (solid dots) from one 50 ps trajectory projected on the $r$–θ plane (defined by the Fe–N distance $r$ and the Fe–N–O angle θ). Also shown is the projection of the entire trajectory onto this plane (dashed line).

The energetic and geometric properties of the crossing configurations from all simulations (a set of 203 crossing events) were used to characterize the transition seam. The height of the rebinding barrier was estimated as follows. For each trajectory the minimum energy $E_{min}$ encountered during this trajectory was used as the reference energy. The height of the barrier was then calculated as the energy difference between $E_{min}$ and the energy at the beginning of a crossing event. The average barrier height over all crossing events was $V = 1.2 \pm 0.4$ kcal/mol. This result is very similar to the experimental estimates (based on the time-dependent barrier model [8]) of 1.2 kcal/mol in MbNO and 1.5 kcal/mol in HbNO. Such a low barrier height is in accordance with the rapid rebinding reaction of NO to myoglobin.

Fig. 12 shows all the configurations for one 50-ps trajectory during which the energy on the bound state surface is less than the energy on the unbound state, projected on the $r-\theta$-plane defined by the Fe–N distance $r$ and the Fe–N–O angle θ (see Fig. 1). The crossing points are shown together with a projection of a trajectory onto the same plane. The expected correlation between the two co-ordinates is manifest from the diagonal shape of the trajectory in this projection. Crossing occurs only if the Fe–N distance is smaller than 4 Å (along the trajectories this distance varies between 3 and 5.5 Å); the average Fe–N distance for crossing was $3.25 \pm 0.25$ Å. A similar localization is seen in the Fe–N–O angle co-ordinate. The dissociated ligand can adopt any orientation along its trajectory but curve crossing occurs only in the vicinity of the native configuration ($\theta = 140°$). The average Fe–N–O angle at a crossing event was $\theta = 136 \pm 12°$ perhaps partly influenced by the harmonic potential used for this angle (see above). It is interesting to note that both the average barrier height ($1.20 \pm 0.40$ kcal/mol) and the average Fe–N distances ($3.25 \pm 0.25$ Å) obtained from the present dynamical calculations on a multi-dimensional potential are similar to the values obtained by Li et al. [18] (1.7 kcal/mol and 3.5 Å).

We did not find any correlation between the barrier crossing points and the total kinetic energy

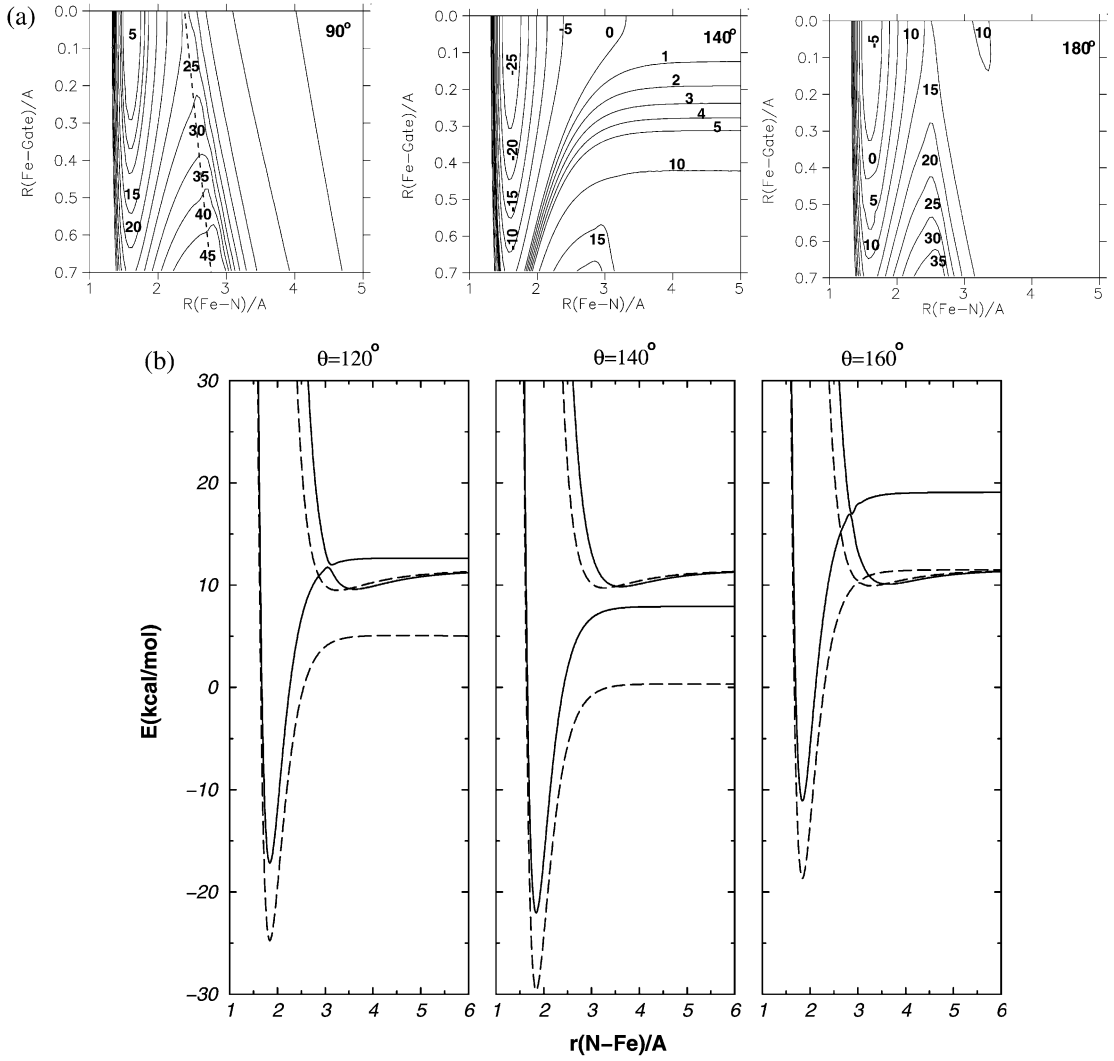


Fig. 13. (a) The adiabatic potential energy surface from a model calculation of the sub-system shown in Fig. 1. $R$(Fe–N) is the distance of the ligands N atom from the iron atom and $R$(Fe-Gate) the distance of the Fe atom from the center of the four pyrrole nitrogens Np. This model shows that as the Fe atom moves out of plane (the Q co-ordinate) the barrier height increases. Potential energy surfaces are shown for three orientations of the NO molecule with respect to the pyrrole plane as indicated in the upper (right-hand curve (90°, 140°, 180°). The transition seam is indicated as the dashed line in the top panel. (b) The two adiabatic curves for the angles θ(Fe–N–O) equal to 120, 140 and 160°. Dashed lines for Fe in the porphyrin plane [$R$(Fe-Gate)=0 in Fig. 13a]; solid lines for Fe out of the porphyrin plane [$R$(Fe-Gate)=0.4 Å in Fig. 13a].

of the NO ligand. The average ligand kinetic energy at the crossing points was $2.8 \pm 1.5$ kcal/mol which is in the range of $1.8 \pm 1.0 - 3.2 \pm 1.6$ kcal/mol found in the full trajectories (not including the initial dissociation). Other co-ordinates and energies that were found to be uncorrelated to the MbNO rebinding barriers include the variation in the kinetic energy of the iron atom (which is thermalized $\frac{3}{2}kT$), the N–O distance and the kinetic energy in the stretching mode, the iron distance

from the heme planes (both the nitrogen plane and the heavy atom plane) and the ligands rotation and center-of-mass translation kinetic energies.

To examine the potential energy underlying the transition seam, we show the results of a model calculation in Fig. 13a,b. To simplify the analysis only two co-ordinates are varied; they are the Fe–N distance and the distance of the Fe atom from the center of the heme plane defined by the four pyrrole nitrogen atoms, Np. All other co-ordinates were fixed at the minimized structure of MbNO. In Fig. 13a, the results obtained with the NO molecule oriented in three different ways are shown: parallel to the pyrrole plane (90°); in the equilibrium configuration (140°) and along the N$\varepsilon$2–Fe–NO axis (180°) (see also Fig. 1). The figures show the adiabatic potential energy surface, which is the lower of the bound-state and unbound-state energies for each configuration, as given by Eqs. (3) and (4), respectively. As the Fe atom moves out-of-plane [increasing R(Fe-Gate)] the barrier height increases. The transition seam is the ridge that runs parallel to the *y*-axis in Fig. 13a (top panel). Regions where a bound well is formed [usually $R$(Fe–N) < 2.0 Å] correspond to configurations on the Morse potential, whereas regions for large values of $R$ (Fe–N) are associated with the unbound potential energy surface. For the planar case [$R$(Fe-Gate) = 0], Fig. 13a shows that as $R$ (Fe–N) decreases for 90° a barrier of approximately 25 kcal/mol appears before the energy drops to approximately 5 kcal/mol to form a bound state with a highly distorted θ(Fe–N–O) angle. For the equilibrium value of θ(Fe–N–O), which corresponds to θ = 140°, there is no barrier while for 180° a slightly more complex situation occurs. Here, the potential energy surface has a first barrier at long range [$R$(Fe–N) ≅ 3.2 Å) and a second barrier at closer Fe–N separations [$R$(Fe–N) ≅ 2.4 Å) before the NO is bound by 5 kcal/mol to the Fe. Thus, the motion of the Fe atom with respect to the pyrrole plane corresponds to a 'gating mode' for the rebinding process; i.e. depending upon the relative position of the iron atom relative to the pyrrole Np atoms rebinding is enhanced or suppressed. These results in Fig. 13a are consistent with the angular range θ = 135 ± 15° sampled by the reactive trajectories (see Fig. 12).

It is instructive to consider one-dimensional cuts through both adiabatic potential energy surfaces for orientations that are important for the rebinding dynamics (Fig. 12). In Fig. 13b the lower and upper adiabats are shown for the Fe atom in the porphyrin plane and at a distance of 0.4 Å from it. In each case, curves for θ(Fe–N–O) equal to 120, 140 and 160° are shown. The middle panel (θ = 140°) shows that for this case the bound state surface is always lower in energy than the unbound surface; i.e. no curve crossing occurs. However, as the Fe atom moves away from the porphyrin plane the distance between the two potential energy curves decreases significantly. For θ = 120° a curve crossing occurs as the Fe atom relaxes out of the porphyrin plane [$R$(Fe–N) ≅ 3.0 Å], which is the preferred position in the unbound state; the adiabatic rebinding barrier is 2 kcal/mol. In the case of θ = 160° both positions of the Fe atom lead to a curve crossing. The out-of-plane position of the Fe atom has a barrier of approximately 6 kcal/mol. It should be noted that all the curves are constructed with the rest of the protein fixed. During the dynamics changes in the protein environment can also lead to changes in these adiabatic potential energy curves, but we have not included this aspect in the model calculations.

### *3.4. Time dependence of rebinding barrier*

Experiments show that the MbNO rebinding kinetics is non-exponential [35]. Two processes have been considered as possible sources for the non-exponential rebinding in MbNO (see Introduction): (a) a time-dependent rebinding barrier; and (b) multiple rebinding barriers, involving several pocket 'trapping' sites [8]. Also, it has been suggested that the non-exponential behavior may be due to trapping of the ligand in secondary pockets. A theoretical study suggested that part of the NO population may be trapped in a distant pocket (behind L29) and contribute to the slower non-exponential rebinding tail [9,18]. This appears to be inconsistent with the original multiflash experiments of Austin et al. [1]. We investigate the possibility that the barrier is time-dependent, as described by Petrich et al. [8].

Examination of the barrier region suggests that the relaxation of the iron position after photodissociation should cause the rebinding barrier to increase with time. Referring to Fig. 2, the rebinding barrier is formed at the crossing between the repulsive unbound potential and the attractive bound potential. Although both curves account for interactions between the ligand and the heme group, these interactions differ in their specific reference frames. While the bound state Morse potential is defined relative to the position of the iron atom (Fe reference frame), the unbound repulsive potential comes mainly from interactions with the four pyrrole nitrogen atoms (pyrrole reference frame). During the relaxation the iron atom moves away from the plane defined by the pyrrole nitrogens. This results in a relative motion of the 'Fe reference frame' with regard to the 'pyrrole reference frame'. The out-of-plane relaxation of the Fe atom causes the two potential curves to move relative to each other. Thus, the position of the intersection between the two surfaces (see Fig. 2) changes as well, as described above.

To determine whether there is a time-dependent increase of the barrier in the MbNO system, we used the molecular dynamics simulations. Specifically, we monitored the time interval between every pair of successive crossing events along a trajectory, and collected their distribution as a function of the time of the first crossing event. The time evolution of this distribution reflects the barrier height time dependence, if any. If the barrier is time independent then the distribution of time intervals between successive crossing events should be independent of the time interval. On the other hand, if the barrier height increases with time, the average interval between successive crossing events should increase, shifting the distribution towards larger values.

Analyzing all possible crossing events found in the 20 simulations (each 50 ps in duration), we calculated the distribution of time intervals between successive events in two time ranges: 0–25 ps; and 25–50 ps. Recrossing events at very early times (0 to approx. 2 ps) are clearly influenced by relaxation of the protein after photodissociation. However, excluding these early recrossings does not change the distribution of

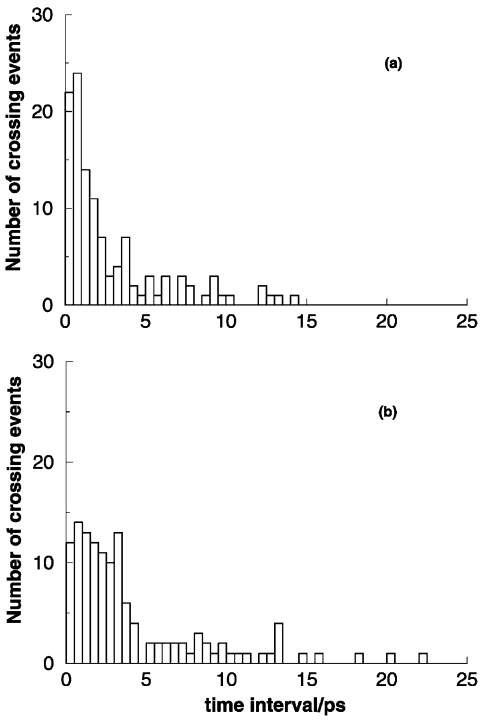


Fig. 14. The distribution of time intervals between successive possible barrier crossings. The distributions are based on all 50 ps RMD trajectories. (a) Short times (0–25 ps) and (b) at longer times (25–50 ps).

transition times because all of these recrossings happen on a very short time scale (50–100 fs). Typically, 2 ps are required to cool the system to the simulation temperature (300 K). Fig. 14 shows the distribution of time intervals between successive barrier crossings. It compares the distribution at early times (0–25 ps; 97 events) with that at later times (25–50 ps; 106 events). Although the distribution does not change its overall shape there is a clear shift towards larger values at longer simulation times. This shift is evident when comparing the average interval in the two time ranges. While at early times the average time interval between possible crossing events was $\tau = 2.83$ ps at later times it increased to $\tau = 4.12$ ps. This is an increase of 46%. These results show that the effective rebinding barrier in MbNO increases as a function of time. From the above analysis (e.g. Fig. 13), this results from an increase in the

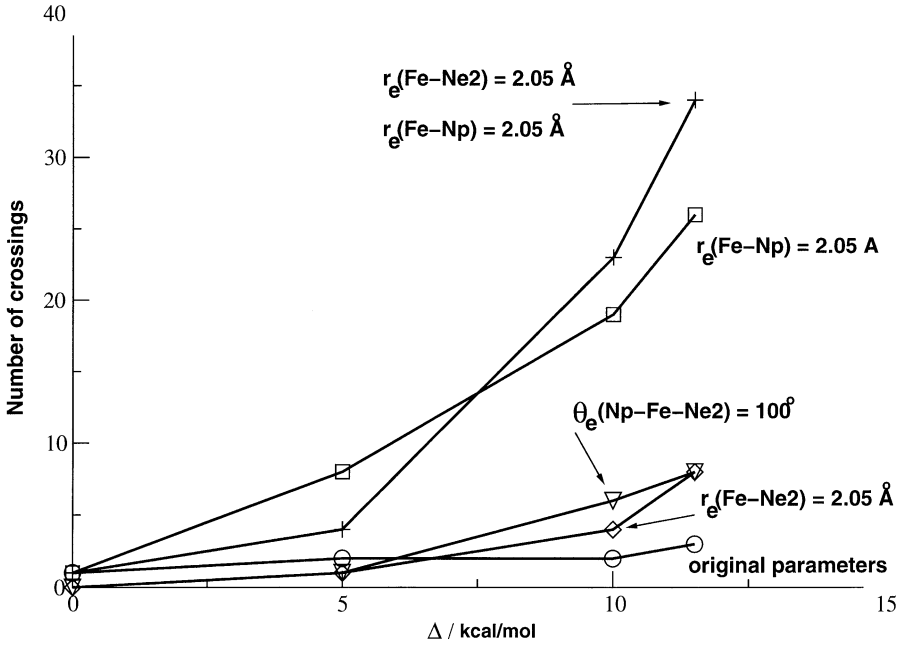


Fig. 15. Sensitivity analysis for the parameters describing the Fe–N$\varepsilon$2 and Fe–$N_P$ distances and the NP–Fe–N$\varepsilon$2 valence angle. The analysis is carried out for the number of crossing events as a function of the asymptotic energy separation $\Delta$ between the bound and unbound potential energy surface. The parameter $\Delta$ corresponds to the splitting between the $^2A$ and $^4A$ potential energy surface at infinite separation (see text). In all five calculations the internal heme parameters have been included in the comparison of the bound and unbound energy. Each curve was calculated using a trajectory 50 ps in length and the initial conditions for all trajectories were identical.

average Fe distance from the porphyrin plane, which in turn, is related to protein relaxation. One is thus led to the conclusion that the time-dependence of the barrier contributes to the non-exponentiality of the rebinding kinetics which takes place on a time scale of approximately 30 ps as suggested by Petrich et al. [8]. This contribution exists in addition to any effects due to the ligand occupying multiple pockets, such as that suggested by Li et al. [18].

## 4. Summary

In this paper we have studied NO rebinding to myoglobin and have focussed on the energetics and structures in the rebinding barrier region. We used the 'Reactive Molecular Dynamics' method in which the system is partitioned into a reaction region and an environment. The system is propagated on the unbound potential energy surface and reactive events are identified by an energy criterion [Eq. (7)]. This approach preserves the high dimensionality of the transition seam at little extra computational cost. A distribution of barrier heights in the range $1.2 \pm 0.4$ kcal/mol was obtained. The fact that such a distribution exists reflects the dynamical character of the rebinding process in that the calculated effective barrier height changes as a result of thermal fluctuations and protein relaxation. Such a distribution is in agreement with experimental estimates for MbNO [5,7,8]. The low barrier leads to rebinding on the times scale of a few picoseconds. A feature which emerges from the simulations is that a collision of the NO with the Fe atom, as such, is not sufficient for them to react. It was found that a region corresponding to the Fe–N distance in the range $3.25 \pm 0.25$ Å and the Fe–N–O angle in the range $136 \pm 12°$ leads to reaction, corresponding to an extended transition seam. The analysis of the time

dependence of the MbNO rebinding barrier clearly indicated that the rebinding barrier is time-dependent, increasing in time as the protein relaxation proceeds over a time scale of tens of picoseconds. This compares well with the estimate of 33 ps from experiment. This time-dependence is likely to be one of the causes of the observed non-exponential rebinding. However, the simulations of Li et al. [18] and Schaad et al. [36] plus the effect of mutants on the rebinding rate, suggest that an additional factor, particularly on longer time scales, may be due to multiple positions of the photodissociated ligand. Further studies into the nature of the relaxation of the system to the bound state are still to be performed. For a quantitative understanding of the energetics and dynamics of the rebinding reaction the interaction between five-coordinated heme and the ligand (here, NO) must be investigated in more detail. Ab initio calculations to do this are in progress.

## Acknowledgments

The authors acknowledge financial support from the Schweizerischer Nationalfonds for an advanced research fellowship (MM) and from the National Institute of Health. We thank Leo Caves and Stefan Fischer for discussions during the period 1992–1994 when part of this work was carried out at Harvard.

## Appendix A: Parametrization for the heme–NO interaction

In this appendix we outline the considerations that were involved in the parameterization for the heme–NO interaction.

1. NO three-point model

In view of previous studies that found that the quadrupole moment is essential for CO dynamics [62], we developed a three-point model for the NO molecule which captures this feature. This model is similar to the CO model developed by Straub and Karplus [17], and reproduces the dipole and quadrupole moments of the molecule as well as ab initio interaction energies of NO with water. The model consists of Lennard–Jones sites and point charges on the N and O atoms, and a point

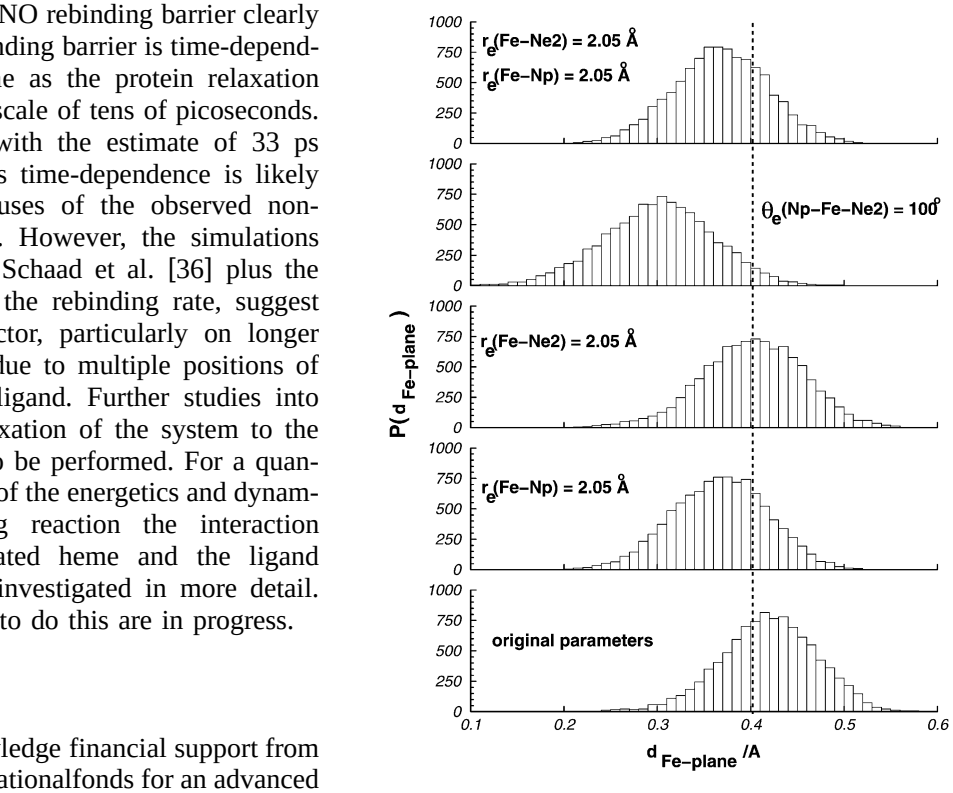


Fig. 16. Distribution of the Fe–N distance for different parameter values. The same trajectories as in Fig. 1b were used. This figure should be compared with Fig. 10.

charge at the center-of-mass. The charge of the center-of mass (which is massless) couples only to the translational motion of the NO molecule and is therefore easily treated in the equations of motion. The forces due to the electrostatic interactions of the protein with the NO center-of-mass charge are distributed to the nitrogen and the oxygen in proportion to the relative masses of the atoms. The three charges were first estimated to give approximate agreement with the experimental dipole moment (0.159 D) and the ab initio quadrupole moment (1.165 DÅ). Then the radii and the charges were slightly refined to fit ab initio quantum mechanical energies for NO interaction with TIP3P water (three configurations). These interactions were obtained by Hartree–Fock calculations with the 6-31G* basis set of the Gaussian98 program [63]. Note, that the charges in the NO model ($-0.25$, 0.595 and $-0.345$) are con-

siderably smaller than those of the equivalent CO model ($-0.75$, 1.6 and $-0.85$), reflecting the smaller quadrupole moment of NO [17].

2. NO bond

Another important feature of this parameterization is that it reflects the fact that NO is a stronger $\pi$-acceptor than CO [64]. This means that the 'back bonding' effect in Fe–NO is stronger than in Fe–CO. As a result, the strengthening of the metal–ligand bond at the expense of the intra-ligand bond is more significant with NO than with CO.

The NO equilibrium bond length was set to 1.141 Å on the basis of crystalline Fe(TPP) (4-MePip) (NO) $CHCl_3$ and in agreement with other six-coordinated heme–model complexes [65–67]. This value is slightly shorter than the equilibrium distance in the gas phase ($r_{eq}=1.1508$ Å [59]). The harmonic force constant [$k$(NO) = 1653 (kcal/mol)/Å$^2$] was chosen to fit a stretching frequency of 1615 cm$^{-1}$ (corresponding to the NO stretching frequency when bound to hemoglobin A ($\nu=1615$ cm$^{-1}$), and in six-coordinated Heme–NO model molecules ($\nu=1625$ cm$^{-1}$) [68].

The values reflect a weakening of the NO bond upon binding: 15% decrease of the stretching frequency (from 1904 cm$^{-1}$ in gas phase [59] to 1615 cm$^{-1}$); and a corresponding 28% weakening of the force constant [from 2295 to 1653 (kcal/mol)/Å$^2$]. These effects are smaller in MbCO, where only a 10% decrease in CO stretching frequency (from 2170 to 1945 cm$^{-1}$), and a 20% weakening of the force constant [from 2736 to 2203 (kcal/mol)/Å$^2$] is observed.

After dissociation, the unbound NO molecule regains its gas phase character, and is described by the gas phase potential. This corresponds to an NO equilibrium distance of $r_{eq}=1.151$ Å, a bond stretching frequency of $\nu_{NO}=1904$ cm$^{-1}$ and a harmonic force constant of $k$(NO) = 2295 (kcal/mol)/Å$^2$ [59].

3. Fe–N bond

This bond, which is broken during the dissociation and reformed during the rebinding event, was modeled by a Morse function. Since we could not find experimental data for the Fe–NO force constant we modeled it based on Fe–CO. Numerous studies have shown that the $\nu$(Fe–C) stretching frequencies in heme proteins and in carbonyl complexes of metalloporphyrins range between 464 and 537 cm$^{-1}$ [69]. Of special relevance are the Fe–C stretching frequencies in different MbCO molecules which are all found to be approximately 510 cm$^{-1}$ [69]. Assuming that the Fe–NO bond is approximately 30% stronger than the Fe–CO bond (NO is a better $\pi$-acceptor than CO) we set the $\nu$(Fe–N) stretching frequency to 663 cm$^{-1}$, with a corresponding harmonic force constant of 696 (kcal/mol)/Å$^2$. For the equilibrium Fe–N distance we chose $r_{eq}=1.740$ Å, based on results for six-coordinated model heme–NO systems [65–67]. To assign the two parameters of the Morse functional form,

$$V = D_e[\exp^{-2\beta(r-r_{eq})} - 2\exp^{-\beta(r-r_{eq})}] \quad (8)$$

i.e. the well depth $D$, and the range parameter $b$, it is necessary to estimate the bond energy for which we use the dissociation energy of NO from Hb ($\approx$30 kcal/mol) [70]. This energy is somewhat larger than the experimental bond energy of MbCO, which is 21.4 kcal/mol [71], and reflect the fact that the Fe–N bond is both deeper and stiffer than the Fe–C bond. The Morse potential parameters that fit the above energy and frequency are: $D_e=30$ kcal/mol; and $\beta=3.2$ Å$^{-1}$. This dissociation energy is also within bounds from recent experimental ($\sim$27 kcal/mol) and theoretical (35 kcal/mol) investigations [72,73].

4. Fe–N–O bond angle

In MbCO the CO axis is tilted relative to the heme-plane and forms an angle with the normal to the plane. However, in the absence of the protein the bond is linear. This bend is attributed to the ligands interaction with the protein [5,74]. For MbNO, however, the situation is somewhat different as NO and $O_2$ form an angle with the normal to the porphyrin plane even in the absence of a protein. Based on data for six-coordinated model heme–NO systems we set the averaged angle to $\theta_{eq}=142°$ [67]. However, when using this value in a harmonic potential energy term, the system equilibrated with a much larger angle of $150\pm4°$. Changing the potential energy parameter to $\theta_{eq}=134°$ and repeating the equilibration resulted in an equilibrated configuration with an equilibrium

angle of $144 \pm 4°$. No further adjustments were applied.

Like all other bond-angles in the CHARMM potential energy the Fe–N–O bending motion is assumed to be harmonic. The force constant was set to 70 (kcal/mol)/rad$^2$, similar to other comparable angles in CHARMM. At thermal energies this force constant allows the angle to fluctuate in a range of $\Delta\theta = \pm 7°$. This is reasonable in view of the fact that in MbCO, the different A-states are defined to $\approx 5$ Å resolution [5].

5. Fe van der Waals parameters

A potentially important interaction on the unliganded potential energy surface is the non-bonded van der Waals interaction between the iron atom and the NO ligand. Following the convention for other van der Waals interactions in CHARMM, this interaction is described in terms of a Lennard–Jones potential. From the 'covalent radius' of the $Fe^{2+}$ ion (1.165 Å), and the 'atomic radius in metals' of Fe (1.23–1.29 Å), we chose to set $r_{\min} = 1.2$ Å [75]. We arbitrarily chose the value $E_{\min} = -0.5$ kcal/mol, which is comparable to energies characterizing other metal atoms. It turned out that these interactions are almost completely masked by the interaction of the ligand with the four pyrrole nitrogens, as the van der Waals minima of the oxygen and nitrogen atom with each of the *N*-pyrrole atom occurs further away than the van der Waals minimum of the Fe–N pair (3.43 vs. 3.30 Å). In other words, the Fe(II) atom is hidden behind the van der Waals spheres of the four *N*-pyrrole atoms.

## Appendix B: Sensitivity of the results to the potential parameters of the unbound state

As mentioned in Section 2.1 the parameters of the unbound (five-coordinated) heme system are less well determined than those for the six-coordinated heme. Therefore, we assessed the changes in the rebinding rate calculated upon modification of the potential parameters. For this analysis, the total unbound ($V_{\text{unbound}} + V^{\text{Heme}}_{\text{unbound}}$) and bound ($V_{\text{bound}} + V^{\text{Heme}}_{\text{bound}}$) potential energies are compared. In this case, the constant $\Delta$ corresponds to the electronic splitting between the $^2A$ and $^4A$ potential energy surface at infinite separation (see Fig. 2). Parameters that were varied included the Np-Fe and N$\varepsilon$2 equilibrium bond lengths $r_e$ and the N$\varepsilon$2–Fe–Np equilibrium bond angle $\theta_e$. The MD simulations with different parameters started from the same structure with the same velocity assignment. The length of each trajectory was 50 ps. Because internal heme parameters are involved, the heme terms $V^{\text{Heme}}_{\text{bound}}$ and $V^{\text{Heme}}_{\text{unbound}}$ mentioned in Section 2.1 are included so that the shift $\Delta$ corresponds to the splitting between the $^2A$ and $^4A$ potential energy surface at infinite separation.

In Fig. 15 the number of crossings for the five cases investigated are shown as a function of the energy splitting $\Delta$ (which is estimated to be 5 kcal/mol) between the $^2$A and $^4$A potential energy surface. However, we show the dependence of the result over a range of $\Delta$ values. The five cases correspond to the original parameter set (see Table 3), the modification $r_e^{\text{Fe–Np}} = 2.05$ Å, the modification $r_e^{\text{Fe–N}\varepsilon 2} = 2.05$ Å, the modification $\theta_e^{\text{Np–Fe–N}\varepsilon 2} = 100°$, and the modification of both $r_e^{\text{Fe–Np}}$ and $r_e^{\text{Fe–N}\varepsilon 2}$ equilibrium distances to 2.05 Å. These changes are of the order of 5% for each parameter. The results in Fig. 5 show that even such moderate changes can have an appreciable influence on the number of recrossings. It is also important to investigate what influence such changes have on the distribution of the Fe–N distances. As is known from experiment, this distance is approximately 0.4 Å. Fig. 16 shows that most simulations give this value. The parameter change which yields a distinctly different Fe–N distance is $\theta_e^{\text{Np–Fe–N}\varepsilon 2}$ for which the average distance is approximately 0.3 Å. Another quantity of interest, which was calculated using the original parameter set, is the value of the constant $\Delta$ as described in Section 2.1. Modification of the Fe–Np equilibrium bondlength to $r_e^{\text{Fe–Np}} = 2.05$ Å, and repeating the calculation from Section 2.1 gives $\Delta = 9.5$ kcal/mol, 2 kcal/mol less than with the original parameter set. Compared to the rather rapid variation of the number of crossings as a function of this parameter, this difference seems small. It indicates that the increase in the number of crossings is not only a 'static' effect but is considerably influenced by rapid, local fluctuations, e.g. due to different restoring forces which arise when potential parameters are varied. These

results suggest that better potential parameters for the five-coordinate heme would be useful for further investigations of Mb–NO.

## References


[1] R. Austin, K. Beeson, L. Eisenstein, H. Frauenfelder, I. Gunsalus, Dynamics of ligand binding to myoglobin, Biochemistry 14 (1975) 5355–5373.

[2] P. Cornelius, R. Hochstrasser, W. Steele, Ultrafast relaxation in picosecond photolysis of Nitrosylhemoglobin, J. Mol. Biol. 163 (1983) 119–128.

[3] J. Martin, A. Migus, C. Poyart, Y. Lecarpentier, R. Astier, A. Antonetti, Femtosecond photolysis of CO-ligated protoheme and hemoproteins: appearance of deoxy species with a 350-fsec time constant, Proc. Natl. Acad. Sci. 80 (1983) 173–177.

[4] A. Ansari, J. Berendzen, S.F. Bowne, et al., Protein states and protein quakes, Proc. Natl. Acad. Sci. 82 (1985) 5000–5004.

[5] A. Ansari, J. Berendzen, D. Braunstein, et al., Rebinding and relaxation in the myoglobin pocket, Biophys. Chem. 26 (1987) 337–355.

[6] P. Anfinrud, C. Han, R. Hochstrasser, Direct observations of ligand dynamics in hemoglobin by subpicosecond infrared spectroscopy, Proc. Natl. Acad. Sci. 86 (1989) 8387–8391.

[7] P.J. Steinbach, A. Ansari, J. Berendzen, et al., Ligand binding to heme proteins: the connection between protein dynamics and function, Biochemistry 30 (1991) 3988–4001.

[8] J.W. Petrich, J.-C. Lambry, K. Kuczera, M. Karplus, C. Poyart, J.-L. Martin, Ligand binding and protein relaxation in heme proteins: a room temperature analysis of NO geminate recombination, Biochemistry 30 (1991) 3975–3987.

[9] Q.H. Gibson, R. Regan, R. Elber, J.S. Olson, T.E. Carver, Distal pocket residues affect picosecond ligand recombination in myoglobin, J. Biol. Chem. 267 (1992) 22022–22034.

[10] J.A. McCammon, S.C. Harvey, Dynamics of Proteins and Nucleic Acids, Cambridge University Press, Cambridge, 1987.

[11] C.L. Brooks, M. Karplus, B.M. Pettitt, Proteins: a Theoretical Perspective of Dynamics, Structure and Thermodynamics, John Wiley & Sons, New York, 1988.

[12] N. Agmon, J. Hopfield, CO binding to heme proteins: a model for barrier height distributions and slow conformational changes, J. Chem. Phys. 79 (1983) 2042–2053.

[13] E. Henry, M. Levitt, W. Eaton, Molecular dynamics simulation of photodissociation of carbon monoxide from hemoglobin, Proc. Natl. Acad. Sci. 82 (1985) 2034–2038.

[14] V. Ŝrajer, L. Reinisch, P. Champion, Protein fluctuations, distributed coupling, and the binding of ligands to heme proteins, J. Am. Chem. Soc. 110 (1988) 6656–6670.

[15] J. Smith, K. Kuczera, M. Karplus, Dynamics of myoglobin: comparison of simulation results with neutron scattering spectra, Proc. Natl. Acad. Sci. 87 (1990) 1601–1605.

[16] R. Elber, M. Karplus, Enhanced sampling in molecular dynamics: use of the time-dependent Hartree approximation for a simulation of carbon monoxide diffusion through myoglobin, J. Am. Chem. Soc. 112 (1990) 9161–9175.

[17] J. Straub, M. Karplus, Molecular dynamics study of the photodissociation of carbon monoxide from myoglobin: ligand dynamics in the first 10 ps, Chem. Phys. 158 (1991) 221–248.

[18] H. Li, R. Elber, J. Straub, Molecular dynamics simulation of NO recombination to myoglobin mutants, J. Biol. Chem. 268 (1993) 17908–17916.

[19] N. Agnion, S. Rabinovich, Non-equilibrium CO binding to heme proteins, J. Chem. Phys. 97 (1992) 7270–7286.

[20] T. Dawson, V. Dawson, S. Snyder, Molecular mechanisms of nitric oxide actions in the brain, Ann. Neurol. 32 (1992) 297–311.

[21] S. Snyder, D. Bredt, Biological roles of nitric oxide, Sci. Am. 266 (5) (1992) 68–71.

[22] T. Traylor, V. Sharma, Why NO?, Biochemistry 31 (1992) 2847–2849.

[23] J. Kuriyan, S. Wilz, M. Karplus, G. Petsko, X-Ray structure and refinement of carbon-monoxy (Fe II)-myoglobin at 1.5 resolution, J. Mol. Biol. 192 (1986) 133–154.

[24] M.F. Perutz, Stereochemistry of cooperative effects in haemoglobin, Nature 228 (1970) 726–739.

[25] B.R. Gelin, M. Karplus, Hemoglobin tertiary structural change on ligand binding: its role in the co-operative mechanism, J. Mol. Biol. 171 (1983) 489–559.

[26] M.F. Perutz, Mechanisms of cooperativity and allosteric regulation in proteins, Q. Rev. Biophys. 22 (1989) 139–237.

[27] M. Karplus, Aspects of protein reaction dynamics: deviations from simple behavior, J. Phys. Chem. B 104 (2000) 11–27.

[28] H. Frauenfelder, N. Alberding, A. Ansari, et al., Proteins and pressure, J. Phys. Chem. 94 (1990) 1024–1037.

[29] M. Ikeda-Saito, Y. Dou, T. Yonetani, et al., Ligand diffusion in the distal heme pocket of myoglobin. A primary determinant of geminate rebinding, J. Biol. Chem. 268 (1993) 6855–6857.

[30] R. Elber, M. Karplus, Multiple conformational states of proteins: a molecular dynamics analysis of myoglobin, Science 235 (1987) 318–321.

[31] K. Kuczera, J. Kuriyan, M. Karplus, Temperature dependence of the structure and dynamics of myoglobin:

a simulation approach, J. Mol. Biol. 213 (1990) 351–373.
[32] R. Czerminski, R. Elber, Computational studies of ligand diffusion in globins: I. Leghemoglobin, Proteins 10 (1991) 70–80.
[33] K. Kuczera, J.-C. Lambry, J.-L. Martin, M. Karplus, Nonexponential relaxation after ligand dissociation from myoglobin: a molecular dynamics simulation, Proc. Natl. Acad. Sci. 90 (1993) 5805–5807.
[34] D.G. Lambright, S. Balasubramanian, S.G. Boxer, Protein relaxation dynamics in human myoglobin, Chem. Phys. 158 (1991) 249–260.
[35] M. Lim, T.A. Jackson, P.A. Anfinrud, Nonexponential protein relaxation: dynamics of conformational change in myoglobin, Proc. Natl. Acad. Sci. 90 (1993) 5801–5804.
[36] O. Schaad, H.-X. Zhou, A. Szabo, W.A. Eaton, E.R. Henry, Simulation of the kinetics of ligand binding to a protein by molecular dynamics: geminate rebinding of nitric oxide to myoglobin, Proc. Natl. Acad. Sci. 90 (1993) 9547–9551.
[37] A. Warshel, M. Levitt, Theoretical studies of enzymic reactions: dielectric, electrostatic and steric stabilization of the carbonium ion in the reaction of lysozyme, J. Mol. Biol. 103 (1976) 227–249.
[38] U.C. Singh, P.A. Kollman, A combined ab initio quantum mechanical and molecular mechanical method for carrying out simulations on complex molecular systems: applications to the $CH_3Cl + Cl^-$ exchange reaction and gas phase protonation of polyethers, J. Comput. Chem. 7 (1986) 718–730.
[39] M.J. Field, P.A. Bash, M. Karplus, A combined quantum mechanical and molecular mechanical potential for molecular dynamics simulations, J. Comput. Chem. 11 (1990) 700–733.
[40] P.A. Bash, M.J. Field, M. Karplus, Free energy perturbation method for chemical reactions in the condensed phase: a dynamical approach based on a combined quantum and molecular mechanics potential, J. Am. Chem. Soc. 109 (1987) 8092–8094.
[41] A. Warshel, M. Karplus, Semiclassical trajectory approach to photoisomerization, Chem. Phys. Lett. 32 (1975) 11–17.
[42] H. Guo, Q. Cui, W.N. Lipscomb, M. Karplus, Substrate conformational transitions in the active site of chorismate mutase: their role in the catalytic mechanism, Proc. Natl. Acad. Sci. 98 (2001) 9032–9037.
[43] J.C. Tully, R.K. Preston, Trajectory surface hopping approach to nonadiabatic molecular collisions: the reaction of $H^+$ with $D_2$, J. Chem. Phys. 55 (1971) 562–572.
[44] M. Godfrey, M. Karplus, Theoretical investigation of reactive collisions in molecular beams: $K + Br_2$, J. Chem. Phys. 49 (1968) 3602–3609.
[45] J. Aqvist, A. Warshel, Simulation of enzyme reactions using valence bond force fields and other hybrid quantum/classical approaches, Chem. Rev. 93 (1993) 2523–2544.
[46] M. Meuwly, J.M. Hutson, Morphing ab initio potentials: a systematic study of Ne–HF, J. Chem. Phys. 110 (1999) 8338–8347.
[47] K. Tanaka, M. Shirasaka, T. Tanaka, Millimeter-wave spectroscopy of the iron carbonyl radical (FeCO), J. Chem. Phys. 106 (1997) 6820–6824.
[48] J.N. Harvey, DFT computation of the intrinsic barrier to CO geminate recombination with heme compounds, J. Am. Chem. Soc. 122 (2000) 12401–12402.
[49] B.R. Brooks, R.E. Bruccoleri, B.D. Olafson, D.J. States, S. Swaminathan, M. Karplus, CHARMM: a program for macromolecular energy, minimization, and dynamics calculations, J. Comput. Chem. 4 (1983) 187–217.
[50] S. Fischer, M. Karplus, Conjugate peak refinement: an algorithm for finding reaction paths and accurate transition-states in systems with many degrees of freedom, Chem. Phys. Lett. 194 (1992) 252–261.
[51] C.L. Brooks, M. Karplus, Deformable stochastic boundaries in molecular dynamics, J. Chem. Phys. 79 (1983) 6312–6325.
[52] A.T. Brünger, C.L. Brooks, M. Karplus, Active site dynamics of ribonuclease, Proc. Natl. Acad. Sci. 82 (1985) 8458–8462.
[53] C.L. Brooks, M. Karplus, Solvent effects on protein motion and protein effects on solvent motion: dynamics of the active site region of lysozyme, J. Mol. Biol. 208 (1989) 159–181.
[54] W.L. Jorgensen, J.D. Chandrasekhar, J.D. Madura, R.W. Impey, M.L. Klein, Comparison of simple potential functions for simulating liquid water, J. Chem. Phys. 79 (1983) 926–935.
[55] W.V. Van Gunsteren, H.J.C. Berendsen, Algorithms for macromolecular dynamics and constraint dynamics, Mol. Phys. 34 (1977) 1311–1327.
[56] M. Brunori, Q.H. Gibson, Cavities and packing defects in the structural dynamics of myoglobin, EMBO Rep. 2 (2001) 674–679.
[57] D. Vitkup, G.A. Petsko, M. Karplus, A comparison between molecular dynamics and X-ray results for dissociated CO in myoglobin, Nat. Struct. Biol. 4 (1997) 202–208.
[58] J. Vojtechovsky, K. Chu, J. Berendzen, R.B. Sweet, I. Schlichting, Crystal structures of myoglobin–ligand complexes at near-atomic resolution, Biophys. J. 77 (1999) 2153–2174.
[59] K.P. Huber, G. Herzberg, Constants of Diatomic Molecules, Van Nostrand, Princeton, 1962.
[60] C.R. Landis, T. Cleveland, T.K. Firman, Valence bond concepts applied to the molecular mechanics description of molecular shapes. 3. Applications to transition metal alkyls and hydrides, J. Am. Chem. Soc. 120 (1998) 2641–2649.
[61] A.K. Rappé, C.J. Casewit, K.S. Colwell, W.A. Goddard, W.M. Skiff, UFF, a full periodic table force field for molecular mechanics and molecular dynamics simulations, J. Am. Chem. Soc. 114 (1992) 10024–10035.

[62] B.J. Berne, G.D. Harp, On the calculation of time correlation functions, Adv. Chem. Phys. 17 (1970) 63–277.
[63] M.J. Frisch, G.W. Trucks, H.B. Schlegel, et al., Gaussian98, Revision A.2, Gaussian, Inc, Pittsburgh, PA, USA, 1998.
[64] J.H. Huheey, Inorganic Chemistry: Principles of Structure and Reactivity, Harper & Row, New York, 1983.
[65] W.R. Scheidt, M.E. Frisse, Nitrosylmetalloporphyrins. II. Synthesis and molecular stereochemistry of nitrosyl-α,β,γ,δ,-tetraphenylporphinatoiron(ii), J. Am. Chem. Soc. 97 (1975) 17–21.
[66] W.R. Scheidt, P.L. Piciulo, Nitrosylmetalloporphyrins. III. Synthesis and molecular stereochemistry of nitrosyl-α,β,γ,δ,-tetraphenylporphinato (1-methylimidazole) iron (II), J. Am. Chem. Soc. 98 (1976) 1913–1919.
[67] K.M. Vogel, P.M. Kozlowski, M.Z. Zgierski, T.G. Spiro, Determinants of the Fe*X*O ($X$=C, N, O) vibrational frequencies in heme adducts from experiment and density functional theory, J. Am. Chem. Soc. 121 (1999) 9915–9921.
[68] J.C. Maxwell, W.S. Caughey, An infrared study of NO bonding to heme B and hemoglobin A. Evidence for inositol hexaphosphate induced cleavage of proximal histidine to iron bonds, Biochemistry 15 (1976) 388–396.
[69] X.-Y. Li, T.G. Spiro, Is bound CO linear or bent in heme proteins? Evidence from resonance Raman and infrared spectroscopic data, J. Am. Chem. Soc. 110 (1988) 6024–6033.
[70] Q.H. Gibson, F.J.W. Roughton, The kinetics and equilibria of the reactions of nitric oxide with sheep haemoglobin, J. Physiol. 136 (1957) 507–526.
[71] M.H. Keyes, M. Falley, R. Lumry, Studies of heme proteins. II. Preparation and thermodynamic properties of sperm whale myoglobin, J. Am. Chem. Soc. 93 (1971) 2035–2040.
[72] O. Chen, S. Groh, A. Liechty, D.P. Ridge, Binding of nitric oxide to iron(II) porphyrins: radiative association, blackbody infrared radiative dissociation, and gas-phase association equilibrium, J. Am. Chem. Soc. 121 (1999) 11910–11911.
[73] C. Rovira, K. Kunc, J. Hutter, P. Ballone, M. Parrinello, Equilibrium geometries and electronic structure of iron–porphyrin complexes: a density functional study, J. Phys. Chem. A 101 (1997) 8914–8925.
[74] T.G. Spiro, P.M. Kozlowski, Is the CO adduct of myoglobin bent, and does it matter?, Acc. Chem. Res. 34 (2000) 137–144.
[75] J.A. Dean, Lange's Handbook of Chemistry, McGraw-Hill, New York, 1973.